ACS Macro Letters

Letter

pubs.acs.org/macroletters

Topologically Distinct Lamellar Block Copolymer Morphologies Formed by Solvent and Thermal Annealing

Ian P. Campbell, Chunlin He, and Mark P. Stoykovich*

Department of Chemical and Biological Engineering, University of Colorado at Boulder, Boulder, Colorado 80309, United States

S *Supporting Information*

ABSTRACT: Solvent annealing produces ordered assemblies in thin films of block copolymers and, in contrast to uniform thermal annealing, can be used to tune the self-assembled morphology, control the domain orientation with respect to the substrate, and, as demonstrated here, reduce the defect density. The two-dimensional network topology of lamellae self-assembled by polystyrene-*block*-poly(methyl methacrylate) block copolymers in thin films was compared when processed by solvent and thermal annealing techniques. The mixed solvent annealing method described here reduced the overall defect density (e.g., dislocations with PMMA or PS cores) and thus the connectivity of the lamellar domains compared to thermal annealing; however, the long-range continuity of the networks was maintained and depended primarily on the copolymer composition. In addition, the persistence length of the lamellar domains for solvent annealed films was found to be 2−3 times that of the corresponding thermally annealed systems.

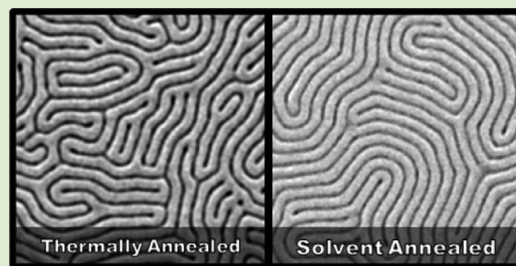

Block copolymer lithography is an emerging nanopatterning technology with capabilities that may complement and eventually replace those provided by existing optical lithography techniques.[1−7] Lithographically relevant morphologies formed by block copolymers in thin films include lamellae and hexagonally close packed cylinder arrays. The perpendicular orientations of these morphologies with respect to the substrate are vital for lithographic applications and can be achieved through approaches including surface modifications (e.g., "neutral" wetting surfaces)[8,9] and directional fields.[10−12] Block copolymer nanostructures with perpendicular orientations possess domains with continuous pathways from the top surface to the bottom surface of the film and, upon selective removal of a copolymer domain, can serve as templates for modifying the substrate through standard additive or subtractive microfabrication processes such as deposition or etching.[13−21] Lamellar-forming block copolymers in thin films with domain orientations perpendicular to the substrate adopt the characteristic "fingerprint" morphology, in which a high-density of energetically unfavorable dislocation and disclination defects leads to linear structures that lack long-range order and have short persistence lengths. These structural defects are not effectively annihilated during self-assembly, and the presence of 3-fold branch points can lead to the formation of highly interconnected and continuous two-dimensional network topologies. The continuity of lamellar networks in 2D is related to the types of defects that are present, with the relative population of defects that connect lamellae determining which domain is continuous. The connectivity of the network is determined by the defect density, with high defect densities resulting in an increased number of connections between adjacent lamellae. We have recently shown that the lamellar morphology and defect structures in thin films are sensitive to the block copolymer composition. The continuity of the block copolymer domains is determined by the copolymer's composition relative to the point of zero spontaneous curvature, with the minority domain inhabiting most defect cores and the majority domain forming defects or branches that connect adjacent lamellae.[22−24] The areal density of defects is limited by the kinetics of defect annihilation, which are exceedingly slow relative to the kinetics of self-assembly for lamellar systems. Increased defect densities and lamellar interconnections provided by branching defects combine to raise the connectivity of the networks such that a lamellar-forming block copolymer can form a continuous network that spans arbitrarily large areas.[24]

Although thermal annealing can produce well-ordered, low-defect films through the use of temperature gradients[25,26] and topological features,[27] solvent annealing has gained favor as a means to rapidly produce order in block copolymer thin films and, in contrast to thermal annealing without gradients, can also be used to control the morphology and orientation of the domains.[28,29] During a typical solvent annealing process, block copolymer thin films are exposed to solvent vapor that permeates and swells the polymer domains to a specified extent, at which point the solvent is removed.[30,31] Order is achieved through the increased mobility of the polymer chains by a plasticization effect (effectively reducing T_g)[32] and reduction of the interaction parameter (χ) through dilution of the polymer chains.[33] There is evidence that the rate at which the solvent is removed, the extent of swelling, the choice

Received: May 30, 2013
Accepted: September 24, 2013
Published: September 27, 2013

 © 2013 American Chemical Society

of solvents, and other process parameters each play important roles in the structures achieved by solvent annealing.[28,34−44] Different solvent annealing conditions to self-assemble the lamellar morphology in thin films can therefore be expected to generate networks with subtle differences in defect structure, defect density, and continuity, due in part to the processing conditions. For example, Ryu and co-workers[45] have shown that solvent annealing using tetrahydrofuran is an effective route to produce order and reduce the defect density in lamellae formed by high molecular weight (256−1000 kg mol^{-1}) block copolymers, although the continuity of the lamellar domains was not characterized.

In this work, the 2D network topology of the lamellar morphology is characterized and compared for the two most important approaches for processing block copolymers in thin films: solvent annealing and thermal annealing. Lamellae formed by poly(styrene-*block*-methyl methacrylate) (PS-*b*-PMMA) copolymers were processed thermally at 190 °C or in a saturated vapor of mixed near-theta solvents (i.e., a mixture of cyclohexane and acetone). The network structures formed by solvent annealing are found to have lower defect densities and longer persistence lengths, as compared to thermal annealing, but the relative defect populations remain sufficient to maintain long-range continuity of the lamellar domains. In addition, processing by solvent annealing is found to not influence the effect of the block copolymer composition on lamellar continuity over large areas, with the volumetric majority domain forming substrate-spanning continuous networks.

Figure 1a,b compare the differences in PS-*b*-PMMA lamellae processed by thermal annealing and solvent annealing, respectively. The annealing process used to self-assemble lamellar-forming block copolymers has a significant effect on the resulting defect density of the networks. The thermally annealed morphology is more tortuous and has a higher defect density than the solvent annealed sample. During solvent annealing, the increased mobility of polymer chains and decreased interaction parameter due to dilution of the chains reduces the energetic barrier for defect annihilation via a melt mechanism.[33,46] Defect annihilation of an isolated dislocation requires a glide mechanism during thermal annealing and will create additional interfacial area. A good comparison of the relative lowering of the barrier for defect annihilation between thermal and solvent annealing can therefore be achieved by estimating the difference in interfacial energies between the defect and the transition state during defect annihilation. The effective interaction parameter can be calculated from the polymer volume fraction in the diluted system (ϕ_p), the polymer−polymer interaction parameter (χ_{AB}), and polymer−solvent interaction parameters ($\chi_{A\text{-solvent}}$, $\chi_{B\text{-solvent}}$; $\chi = [\chi_{AB} + \chi_{A\text{-solvent}} - \chi_{B\text{-solvent}}]\phi_p$ for a slight to moderate addition of a third, solvent component).[33] In the case here of symmetric swelling by solvents preferentially partitioned between domains and a mixture of near-theta solvents, $\chi_{A\text{-solvent1}} \approx \chi_{B\text{-solvent2}} \approx 0$ and leads to a simple dilution equation for χ based on the polymer volume fraction ($\chi = \chi_{AB}\,\phi_p$).[33] The free energy of the polymer interface can be calculated as $F_{int}/k_bT = \rho_o Aa(\chi/6)^{1/2}$, assuming no entropic contributions, where ρ_o is the inverse molecular specific volume, A is the interfacial area per block copolymer molecule, and a is the statistical segment length.[47] As the polymer domains swell during solvent annealing, the interfacial area per molecule should increase in proportion to the decrease in inverse specific volume, leading to an interfacial energy solely dependent on χ. During solvent annealing, the final swollen state is ~3 times the initial film volume, leading to a dilution of $\chi \approx \chi_{AB}/3$ and an interfacial energy barrier for defect annihilation of approximately 57% that of the pure block copolymer in the thermal melt state. Beyond the reduced energy barrier, defect annihilation via a melt mechanism is also facilitated by increased diffusion of the polymer chains perpendicular to the polymer−polymer interface in the swollen state. Reduced χ through solvent molecule infiltration and increased polymer plasticization during solvent annealing leads to a dramatic increase in the diffusion coefficient perpendicular to lamellar interfaces during solvent annealing compared to thermal annealing.[48] With an increased diffusion coefficient, the barrier to diffusion across lamellar interfaces is effectively eliminated and leads to rapid defect annihilation at near-zero activation energy.[46] This defect annihilation mechanism is kinetically prohibited in the thermal melt for our system ($\chi N \approx 37$) because of the high diffusion barrier and leads to stable defect populations at long annealing times. A noticeable number of defects also remain after solvent annealing even though the activation barrier is dramatically reduced, due likely

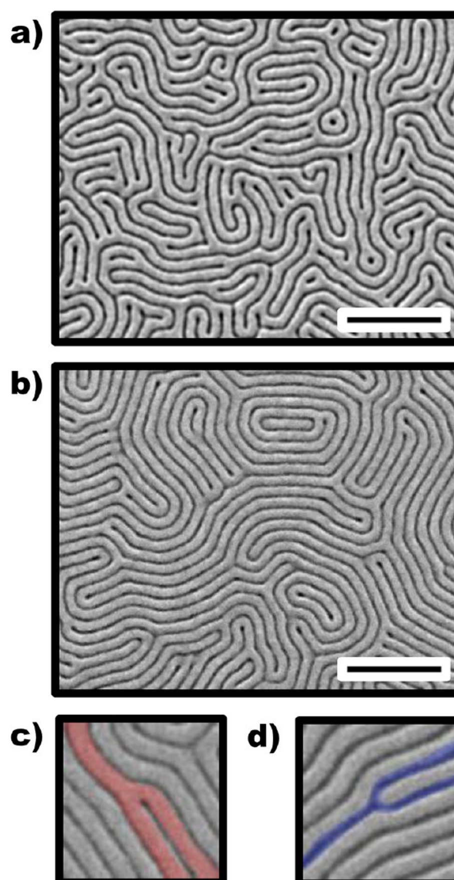

Figure 1. Scanning electron micrographs comparison of lamellar morphologies that were (a) thermally annealed and (b) solvent annealed in PS-*b*-PMMA (53k:54k) thin films. The light and dark domains correspond to the PS and PMMA domains, respectively. The reduced defect density in the solvent annealed sample dramatically decreases the connectivity of the network while maintaining similar continuity. Connectivity in these images is primarily due to branches in the lamellae that occur through (c) PMMA core dislocation and (d) PS core dislocation defects. The red and blue highlights illustrate the increased connectivity in the PS and PMMA domains, respectively. The scale bars correspond to 400 nm.

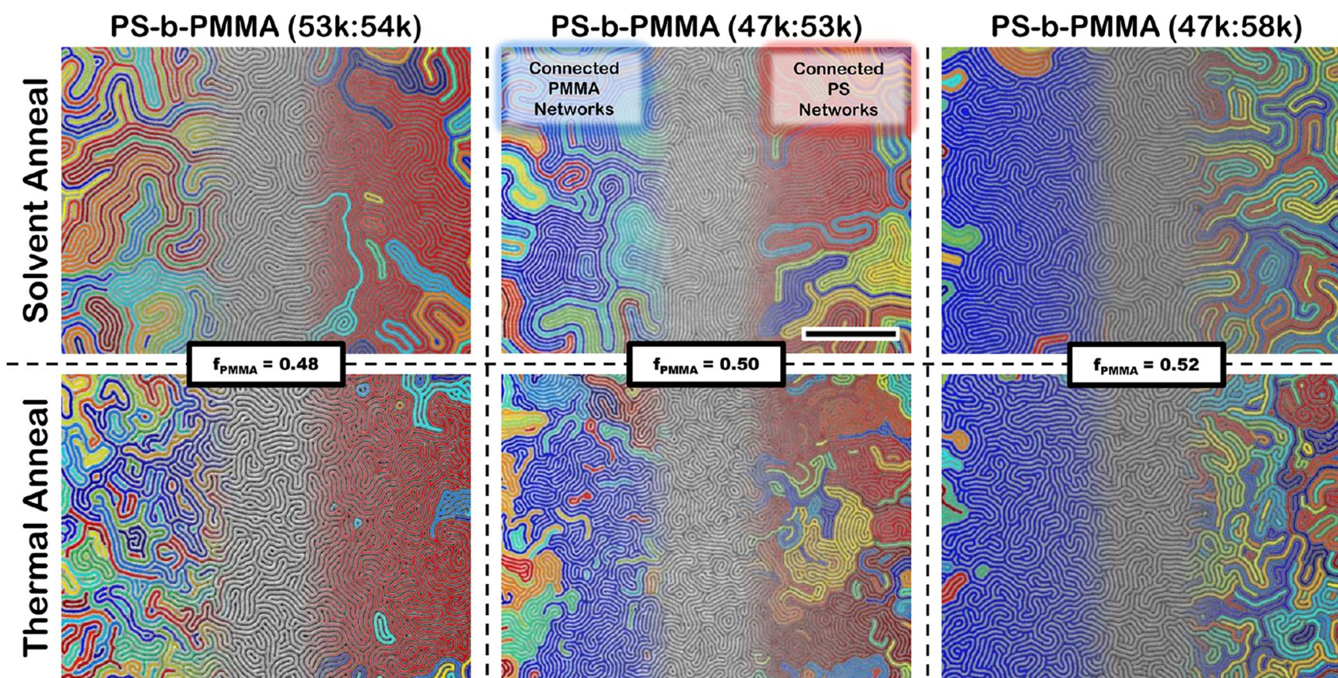

Figure 2. Comparison between thermal and solvent annealing across a range of block copolymer compositions. Colorized continuous networks of PMMA and PS are overlaid on the left and right sides of the individual SEM images (unmodified in the middle), respectively. Each individually colored network represents an isolated, continuous network, although networks on the image border may be connected outside the imaged area. There is a transition in continuity from PS to PMMA as the volume fraction of PMMA is increased from f_{PMMA} = 0.48−0.52. Increasing asymmetry in the composition incorporates larger fractions of the continuous lamellae in a substrate-spanning network. The scale bar corresponds to 1 μm for all images.

to a low energy difference between the single-crystalline and defective morphologies which causes a Boltzmann distribution of defect states.

The PMMA core dislocation defect is the most common defect observed in the lamellar morphologies in Figure 1a,b and is shown magnified in Figure 1c. This defect type connects adjacent PS lamellae, helps to form continuous PS networks, and subdivides a PMMA lamella into two distinct segments. Previously, ~70% of the defects in a PS-*b*-PMMA lamellar system with a volume fraction of PMMA of f_{PMMA} = 0.49 were found to be PMMA core dislocations.[49] The block copolymer used to form the networks in Figure 1a,b has f_{PMMA} = 0.48 and, thus, also forms large populations of PMMA core dislocations. This observation is consistent with work that has shown that the domain continuity of PS-*b*-PMMA is dependent on the composition in relation to the point of zero spontaneous curvature.[24] Increasing compositional asymmetry further imbalances the relative population of PS core and PMMA core dislocation defects, and results in improved connectivity for the continuous domain. A highly asymmetric composition forming well-connected PS domains has a larger fraction of PMMA core dislocation defects relative to the total defect population, as compared to a less asymmetric composition that still forms continuous PS networks. When the block copolymer composition is shifted to the other side of the point of zero spontaneous curvature, which for PS-*b*-PMMA lies at $f_{PMMA} \approx$ 0.51,[50−52] the most common defect type is the PS core dislocation, shown in Figure 1d, which favors PMMA domain continuity and connectivity. The PS core dislocation defect connects neighboring PMMA lamellae and produces a well-connected, continuous, PMMA network.

Figure 2a compares the structures achieved by thermal and solvent annealing across a range of PS-*b*-PMMA block copolymer compositions. The connected networks for PMMA and PS are colorized and overlaid on the left and right sides, respectively, of the original SEM images. Each individually colored network represents a distinct structure that can be traced without crossing the other domain. Some colors are repeated due to a limited color palette and networks on the image border may be connected to the largest network outside the imaged area. With $f_{PMMA} \approx$ 0.48 (PS-*b*-PMMA, 53k:54k), both thermal and solvent annealing produce a large red PS network that spans the entire imaged area. However, the reduced defect density that results from solvent annealing led to decreased lamellar connectivity. With fewer defects, such as the PMMA core dislocations, there are not as many connections between neighboring PS lamellae and there is less redundancy in the pathways that form the network, thereby increasing the chance of forming isolated networks. Solvent annealing also results in fewer PS branches to subdivide the PMMA domains and the PMMA lamellae form larger continuous structures, though none of them are continuous across the imaged area. A more compositionally symmetric system at $f_{PMMA} \approx$ 0.50 (PS-*b*-PMMA, 47k:53k) formed large networks in both the PS and PMMA domain. This composition is very close to the point of zero spontaneous curvature at $f_{PMMA} \approx$ 0.51, and while the PS domain should in theory be continuous, the reduced connectivity made it impossible to image large enough areas to infer the topology over the entire substrate and it appears that the PMMA continuity was slightly favored. Additionally, the point of zero spontaneous curvature is calculated at the strong segregation limit and will shift toward symmetric volume fractions with decreasing χN, creating larger networks of both PS and PMMA that may be locally bicontinuous when $f_{PMMA} \approx$ 0.50. Shifting the copolymer composition to the other side of the point of zero spontaneous

curvature at $f_{PMMA} \approx 0.52$ (PS-*b*-PMMA, 47k:58k) produced a continuous blue PMMA network for both thermal and solvent annealing. Each block copolymer had a network continuity that was independent of whether it was annealed by solvent or thermal processing, implying that all types of defects are equally reduced in density through solvent annealing. This observation therefore suggests that the domains are swollen symmetrically by the mixed solvent vapor used here, which is not an unreasonable expectation given that the cyclohexane and acetone solvents are nearly θ solvents for the PS and PMMA domains, respectively, at the processing conditions.

The densities of branch and end points in the network after processing by thermal or solvent annealing are quantified in Figure 3 for the three block copolymer compositions. The branch and end point densities for solvent annealed samples are significantly lower (>2-fold) than those for thermally annealed samples. There is also a clear trend in the branch and end point densities as a function of copolymer composition; as the composition becomes more asymmetric, the branch point density for the continuous majority domain and the end point density in the minority domain increase. This is coupled with a decrease in end point density in the continuous domain and a concomitant decrease in the branch point density of the minority domain. The copolymer composition therefore determines the defect population distribution, and increasing the compositional asymmetry relative to the point of zero spontaneous curvature leads to larger fractions of defects that favor continuity in the majority domain.

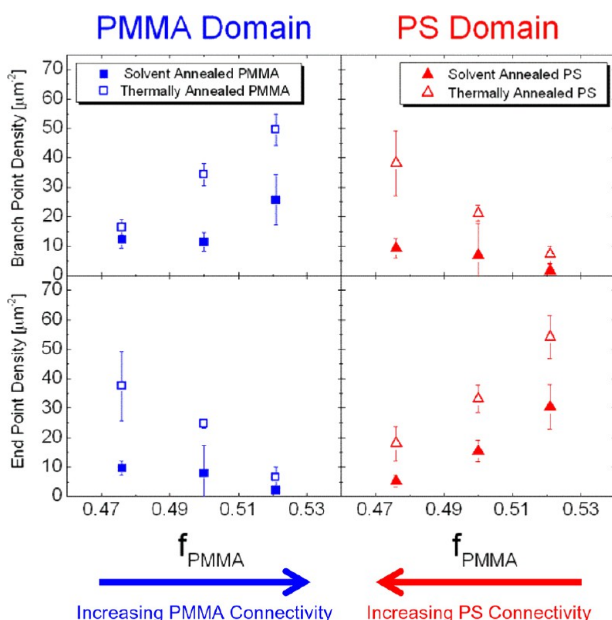

Figure 3. Branch and end point density in the PS-*b*-PMMA lamellar morphologies in thin films for solvent annealed (filled symbols) and thermally annealed (open symbols) samples across a range of compositions. Solvent annealing reduces the lamellar defect density and decreases the branch and end point densities for all compositions. Increasing asymmetry in volume fraction shifts the defect populations to favor branch points and connectivity in the volumetrically favored domain. The error bars correspond to two standard deviations.

Lamellae formed by block copolymer systems during solvent annealing have low defect densities that are also correlated to a decrease in the average interfacial curvature between domains. Long, straight lamellae are observed to form and to be well-aligned with neighboring lamellae. The persistence length can be used to quantify the straightness of the lamellae and measures the distance along a lamellar domain before correlations in direction are lost. Figure 4 shows that PS-*b*-PMMA lamellae that are solvent annealed have 2−3 times the persistence length of thermally annealed lamellae across all compositions, thus, indicating that the direction of the lamellae are correlated over much longer distances. This is consistent with the images shown in Figure 1 that qualitatively show that "straighter" lamellae and lower absolute defect densities are achieved by solvent annealing. It is not the case that lower defect densities must necessarily lead to lamellae with longer persistence lengths; network topologies with high tortuous pathways (lamellae) between network nodes (defects such as branches) can be envisioned for any node density. However, there is a clear correlation between defect density and persistence length in thin film lamellar block copolymer systems, likely due to the ease with which the energetic penalties associated with interfacial bending and deformation can be minimized in comparison to those energies associated with defect annihilation.

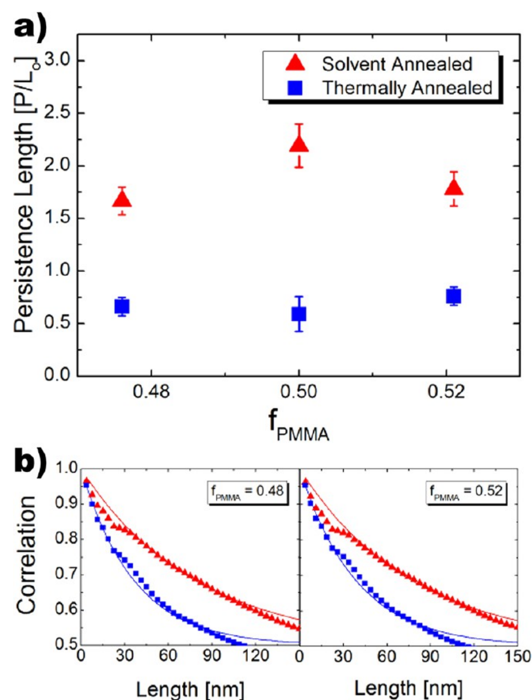

Figure 4. (a) Persistence length of lamellar domains for solvent annealed (red triangles) and thermally annealed (blue squares) PS-*b*-PMMA thin films. Solvent annealing reduces the defect density of all compositions and leads to longer persistence lengths. Error bars correspond to two standard deviations found by linear regression of the fit. (b) Examples of the correlation $\langle\cos(\theta)\rangle$ calculated as a function of lamellar contour length for $f_{PMMA} = 0.48$ (left) and 0.52 (right). The least-squares fits of $\langle\cos(\theta)\rangle = (\exp(-L/P) + 1)/2$ used to calculate the persistence length P are shown as solid curves.

The lamellar morphologies with low-defect densities self-assembled by solvent annealing are found to persist unchanged even upon subsequent thermal annealing, therefore indicating that the lamellar networks are stable and that the processing pathway and history are important. Branch and end-point densities of solvent annealed lamellae that are then thermally processed well above the glass transition temperature remain

unchanged, and the networks do not revert topologically to those formed by thermally annealing (as shown in Figure S2) even over the course of 12 h at 190 °C. This suggests that the increased chain mobility and reduced interaction parameter during solvent annealing facilitate defect annihilation and decrease the system free energy beyond what can be achieved by thermal annealing alone. This stability differs from prior observations of morphology and domain orientation in thin film morphologies trapped during solvent annealing, and suggests that specific solvent annealing conditions are critical for achieving stable lamellar morphologies and low-defect densities. For example, one would expect that asymmetric domain swelling during solvent annealing would lead to lamellar defect populations that are not dependent solely on the composition of the block copolymer and differ from those achieved here under symmetric swelling conditions or by thermal annealing.[38] Such asymmetrically swollen systems are unlikely to be stable and upon subsequent thermal annealing additional defects may be introduced as a result of volumetric frustrations introduced during solvent annealing. The quality of the solvent also plays a role in the resultant lamellar morphology after solvent annealing. Better solvents will enthalpically favor long, straight polymer chains extending away from the interface and thereby increase the domain size compared to thermal annealing.[53] Alongside the domain expansion, good solvents will also reduce the entropic contribution of each chain and when coupled with asymmetric swelling, may lead to interfacial curvatures not exhibited during thermal annealing. Utilizing a binary blend of theta solvents for the block copolymer domains eliminates complications that may result from asymmetric swelling or chain elongation, and allows for subsequent thermal annealing of the solvent annealed morphologies without concern for structural transitions between the equilibrium and trapped morphologies. We have also characterized the stability of a thermally annealed lamellar thin film upon subsequent solvent annealing. In this case the resulting lamellar networks were identical to those solvent annealed and had no memory of the original thermally annealed morphology, perhaps due to rapid defect annihilation.

In conclusion, solvent annealing leads to lamellar morphologies of block copolymers in thin films that are statistically distinct from those self-assembled by thermal annealing. Defect annihilation is facilitated by solvent annealing beyond what is normally achieved by thermal annealing, leading to reductions in the connectivity of the lamellar networks without significant changes in their long-range continuity. The ability to directly control the two-dimensional network topologies in thin films enables tuning the in-plane transport properties of the nanostructures important for engineering applications (e.g., barrier membranes or transparent conductive electrodes).[54−57] Highly interconnected, continuous networks provide redundant pathways and may increase mass or energy flux through parallel transport. The presented work also sheds light on methods that may facilitate further defect annihilation during the directed self-assembly of block copolymers. As the use of block copolymers becomes increasingly widespread due to their compatibility with existing lithographic processes, it is important to ensure perfect registration with guiding templates (e.g., topographic[27,58,59] or chemically patterned surfaces[60]) and extremely low defect densities. By utilizing compositions tuned to match the guiding template and processing conditions that further reduce defect densities, it may be possible to drive the defect density well below the limiting threshold for high performance electronic devices.

■ EXPERIMENTAL METHODS

Substrate Preparation: Silicon wafers were purchased from University Wafer and cleaned using piranha solution. The wafers were then rinsed with deionized water and dried overnight under vacuum. A neutral wetting surface for the block copolymer was created by spincoating a 0.3 wt % solution of random copolymer (PS-*r*-MMA-*r*-GMA, 59 mol % PS, 40 mol % PMMA, 1 mol % glycidyl methacrylate) in toluene (anhydrous, EMD Chemicals, 99.8 wt %) on the wafer and annealing for 4 h at 190 °C.[9,61] Random copolymer that was not cross-linked into the surface treatment layer was removed by sonication in toluene. This surface treatment provided a "neutral" substrate for all of the lamellar-forming PS/PMMA block copolymer systems characterized here, such that there was no preference for PS or PMMA to wet the substrate and perpendicular orientations were achieved.

Thin Film Preparation and Block Copolymer Self-Assembly: PS-continuous block copolymer [polystyrene-*block*-poly(methyl methacrylate) or PS-*b*-PMMA, 53k:54k, PDI = 1.16], PMMA-continuous block copolymer (PS-*b*-PMMA, 47k:58k, PDI = 1.09), and symmetric block copolymer (PS-*b*-PMMA, 47k:53k, PDI = 1.12) were used as purchased from Polymer Source. Individual solutions were prepared by weighing out dry polymer and adding anhydrous toluene to reach the desired weight fraction. Block copolymer solutions were spin-coated onto previously prepared neutral substrates at a thickness 1.1 times the lamellar periodicity (L_o). Self-assembly by thermal annealing was performed by annealing block copolymer thin films under ~2 Torr vacuum at 190 °C for 10 days. Self-assembly by solvent annealing was carried out in a saturated vapor of acetone and cyclohexane. Polymer films were allowed to swell for 270 min to a total thickness of $\sim 3L_o$ before quenching using 200 Torr vacuum. The total time to quench was approximately 3 min. Solvent annealed films were subsequently thermally annealed for 1 h at 190 °C to improve phase separation and to flatten the film. Full details of the solvent annealing procedure are available in the Supporting Information.

Nanostructure Imaging: The block copolymer morphologies were imaged using a JEOL JSM-7401F scanning electron microscope (SEM) operating at a 2 kV accelerating voltage and 1 kV sample bias. The nanostructures observed at the top surface of the film were assumed to propagate through the film to the substrate based on cross-sectional SEM images for similar systems with thicknesses approximately equal to L_o.[60]

Characterization of Lamellar Morphology: The as-collected scanning electron micrographs had their contrast enhanced and were smoothed using the ImageJ software.[62] The lamellar periodicity of the pure block copolymer was determined to be ~51.8 nm (see Figure S1). The lamellar morphology was characterized using an in-house program developed for Matlab (v. R2012a, The Mathworks, Natick, MA). In order to accurately compare the network morphology of the polymers, the branch and end point densities were normalized by the ratio of $(L_{o,\text{PS-}b\text{-PMMA}}/L_{o,53k:54k})^2$ to ensure that the same areas relative to L_o were examined. Additional details of the morphological analysis are available in the literature[24] and the Supporting Information.

■ ASSOCIATED CONTENT

Supporting Information

Details of the solvent annealing procedure, an overview of the network analysis process, the evolution of solvent annealed structures upon additional thermal processing, and Fast Fourier transforms used to determine the periodicity of each polymer. This material is available free of charge via the Internet at http://pubs.acs.org.

■ AUTHOR INFORMATION

Corresponding Author

*E-mail: mark.stoykovich@colorado.edu.

Notes

The authors declare no competing financial interest.

■ ACKNOWLEDGMENTS

This research was supported in part by the NNIN at the Colorado Nanofabrication Laboratory and the National Science Foundation under Grant No. ECS-0335765. This work was performed in part at the University of Colorado's Nanomaterials Characterization Facility.

■ REFERENCES

(1) Park, M.; Harrison, C.; Chaikin, P. M.; Register, R. A.; Adamson, D. H. *Science* **1997**, *276* (5317), 1401–1404.
(2) Whitesides, G. M.; Ostuni, E.; Takayama, S.; Jiang, X. Y.; Ingber, D. E. *Annu. Rev. Biomed. Eng.* **2001**, *3*, 335–373.
(3) Hawker, C. J.; Russell, T. P. *MRS Bull.* **2005**, *30* (12), 952–966.
(4) Stoykovich, M. P.; Nealey, P. F. *Mater. Today* **2006**, *9* (9), 20–29.
(5) Black, C. T. *ACS Nano* **2007**, *1* (3), 147–150.
(6) Black, C. T.; Ruiz, R.; Breyta, G.; Cheng, J. Y.; Colburn, M. E.; Guarini, K. W.; Kim, H. C.; Zhang, Y. *IBM J. Res. Dev.* **2007**, *51* (5), 605–633.
(7) Kim, H. C.; Hinsberg, W. D. *J. Vac. Sci. Technol. A* **2008**, *26* (6), 1369–1382.
(8) Mansky, P.; Liu, Y.; Huang, E.; Russell, T. P.; Hawker, C. J. *Science* **1997**, *275* (5305), 1458–1460.
(9) Ham, S.; Shin, C.; Kim, E.; Ryu, D. Y.; Jeong, U.; Russell, T. P.; Hawker, C. J. *Macromolecules* **2008**, *41* (17), 6431–6437.
(10) Koppi, K. A.; Tirrell, M.; Bates, F. S.; Almdal, K.; Colby, R. H. *J. Phys. II* **1992**, *2* (11), 1941–1959.
(11) Morkved, T. L.; Lu, M.; Urbas, A. M.; Ehrichs, E. E.; Jaeger, H. M.; Mansky, P.; Russell, T. P. *Science* **1996**, *273* (5277), 931–933.
(12) Osuji, C.; Ferreira, P. J.; Mao, G. P.; Ober, C. K.; Vander Sande, J. B.; Thomas, E. L. *Macromolecules* **2004**, *37* (26), 9903–9908.
(13) Cheng, J. Y.; Ross, C. A.; Chan, V. Z. H.; Thomas, E. L.; Lammertink, R. G. H.; Vancso, G. J. *Adv. Mater.* **2001**, *13* (15), 1174–1178.
(14) Gowrishankar, V.; Miller, N.; McGehee, M. D.; Misner, M. J.; Ryu, D. Y.; Russell, T. P.; Drockenmuller, E.; Hawker, C. J. *Thin Solid Films* **2006**, *513* (1–2), 289–294.
(15) Aizawa, M.; Buriak, J. M. *Chem. Mater.* **2007**, *19* (21), 5090–5101.
(16) Liu, C. C.; Nealey, P. F.; Ting, Y. H.; Wendt, A. E. *J. Vac. Sci. Technol. B* **2007**, *25* (6), 1963–1968.
(17) Zschech, D.; Kim, D. H.; Milenin, A. P.; Scholz, R.; Hillebrand, R.; Hawker, C. J.; Russell, T. P.; Steinhart, M.; Gosele, U. *Nano Lett.* **2007**, *7* (6), 1516–1520.
(18) Chai, J.; Buriak, J. M. *ACS Nano* **2008**, *2* (3), 489–501.
(19) Xiao, S. A. G.; Yang, X. M.; Lee, K. Y.; ver der Veerdonk, R. J. M.; Kuo, D.; Russell, T. P. *Nanotechnology* **2011**, *22* (30), 305302.
(20) Park, S.; Lee, D. H.; Xu, J.; Kim, B.; Hong, S. W.; Jeong, U.; Xu, T.; Russell, T. P. *Science* **2009**, *323* (5917), 1030–1033.
(21) Jung, Y. S.; Lee, J. H.; Lee, J. Y.; Ross, C. A. *Nano Lett.* **2010**, *10* (9), 3722–3726.
(22) Matsen, M. W.; Bates, F. S. *J. Polym. Sci., Part B: Polym. Phys.* **1997**, *35* (6), 945–952.
(23) Matsen, M. W. *J. Phys.: Condens. Matter* **2002**, *14* (2), R21–R47.
(24) Campbell, I. P.; Lau, G. J.; Feaver, J. L.; Stoykovich, M. P. *Macromolecules* **2012**, *45* (3), 1587–1594.
(25) Berry, B. C.; Bosse, A. W.; Douglas, J. F.; Jones, R. L.; Karim, A. *Nano Lett.* **2007**, *7* (9), 2789–2794.
(26) Berry, B. C.; Singh, G.; Kim, H.-C.; Karim, A. *ACS Macro Lett.* **2013**, *2* (4), 346–350.
(27) Segalman, R. A.; Yokoyama, H.; Kramer, E. J. *Adv. Mater.* **2001**, *13* (15), 1152–1155.
(28) Ho, R. M.; Tseng, W. H.; Fan, H. W.; Chiang, Y. W.; Lin, C. C.; Ko, B. T.; Huang, B. H. *Polymer* **2005**, *46* (22), 9362–9377.
(29) Phillip, W. A.; Hillmyer, M. A.; Cussler, E. L. *Macromolecules* **2010**, *43* (18), 7763–7770.
(30) Fukunaga, K.; Elbs, H.; Magerle, R.; Krausch, G. *Macromolecules* **2000**, *33* (3), 947–953.
(31) Kim, S. H.; Misner, M. J.; Xu, T.; Kimura, M.; Russell, T. P. *Adv. Mater.* **2004**, *16* (3), 226–231.
(32) Chow, T. S. *Macromolecules* **1980**, *13* (2), 362–364.
(33) Helfand, E.; Tagami, Y. *J. Chem. Phys.* **1972**, *56* (7), 3592–3601.
(34) Xuan, Y.; Peng, J.; Cui, L.; Wang, H. F.; Li, B. Y.; Han, Y. C. *Macromolecules* **2004**, *37* (19), 7301–7307.
(35) Korczagin, I.; Hempenius, M. A.; Fokkink, R. G.; Stuart, M. A. C.; Al-Hussein, M.; Bomans, P. H. H.; Frederik, P. M.; Vancso, G. J. *Macromolecules* **2006**, *39* (6), 2306–2315.
(36) Guo, R.; Huang, H.; Chen, Y.; Gong, Y.; Du, B.; He, T. *Macromolecules* **2008**, *41* (3), 890–900.
(37) Wang, Y.; Hong, X. D.; Liu, B. Q.; Ma, C. Y.; Zhang, C. F. *Macromolecules* **2008**, *41* (15), 5799–5808.
(38) Jung, Y. S.; Ross, C. A. *Adv. Mater.* **2009**, *21* (24), 2540–2545.
(39) Paik, M. Y.; Bosworth, J. K.; Smilges, D.-M.; Schwartz, E. L.; Andre, X.; Ober, C. K. *Macromolecules* **2010**, *43* (9), 4253–4260.
(40) Albert, J. N. L.; Bogart, T. D.; Lewis, R. L.; Beers, K. L.; Fasolka, M. J.; Hutchison, J. B.; Vogt, B. D.; Epps, T. H., III. *Nano Lett.* **2011**, *11* (3), 1351–1357.
(41) Kim, B.; Hong, S. W.; Park, S.; Xu, J.; Hong, S.-K.; Russell, T. P. *Soft Matter* **2011**, *7* (2), 443–447.
(42) Albert, J. N. L.; Young, W.-S.; Lewis, R. L.; Bogart, I. I. I.; Smith, T. D.; Epps, J. R.; III., T. H. *ACS Nano* **2012**, *6* (1), 459–466.
(43) Gotrik, K. W.; Hannon, A. F.; Son, J. G.; Keller, B.; Alexander-Katz, A.; Ross, C. A. *ACS Nano* **2012**, *6* (9), 8052–8059.
(44) Lee, D. H.; Cho, H.; Yoo, S.; Park, S. *J. Colloid Interface Sci.* **2012**, *383*, 118–123.
(45) Kim, E.; Ahn, H.; Park, S.; Lee, H.; Lee, M.; Lee, S.; Kim, T.; Kwak, E.-A.; Lee, J. H.; Lei, X.; Huh, J.; Bang, J.; Lee, B.; Ryu, D. Y. *ACS Nano* **2013**, *7* (3), 1952–1960.
(46) Takahashi, H.; Laachi, N.; Delaney, K. T.; Hur, S.-M.; Weinheimer, C. J.; Shykind, D.; Fredrickson, G. H. *Macromolecules* **2012**, *45* (15), 6253–6265.
(47) Semenov, A. N. *Zh. Eksp. I Teor. Fiz.* **1985**, *88* (4), 1242–1256.
(48) Barrat, J. L.; Fredrickson, G. H. *Macromolecules* **1991**, *24* (24), 6378–6383.
(49) Kim, S. O.; Kim, B. H.; Kim, K.; Koo, C. M.; Stoykovich, M. P.; Nealey, P. F.; Solak, H. H. *Macromolecules* **2006**, *39* (16), 5466–5470.
(50) Kirste, R. G. *Makromol. Chem.* **1967**, *101* (MAR), 91–103.
(51) Ballard, D. G. H.; Wignall, G. D.; Schelten, J. *Eur. Polym. J.* **1973**, *9* (9), 965–969.
(52) Russell, T. P.; Hjelm, R. P.; Seeger, P. A. *Macromolecules* **1990**, *23* (3), 890–893.
(53) Jeong, J. W.; Park, W. I.; Kim, M. J.; Ross, C. A.; Jung, Y. S. *Nano Lett.* **2011**, *11* (10), 4095–4101.
(54) Hu, L.; Hecht, D. S.; Gruner, G. *Nano Lett.* **2004**, *4* (12), 2513–2517.
(55) Singh, M.; Odusanya, O.; Wilmes, G. M.; Eitouni, H. B.; Gomez, E. D.; Patel, A. J.; Chen, V. L.; Park, M. J.; Fragouli, P.; Iatrou, H.; Hadjichristidis, N.; Cookson, D.; Balsara, N. P. *Macromolecules* **2007**, *40* (13), 4578–4585.
(56) Kocabas, C.; Pimparkar, N.; Yesilyurt, O.; Kang, S. J.; Alam, M. A.; Rogers, J. A. *Nano Lett.* **2007**, *7* (5), 1195–1202.
(57) Jha, A. K.; Chen, L.; Offeman, R. D.; Balsara, N. P. *J. Membr. Sci.* **2011**, *373* (1–2), 112–120.
(58) Jung, Y. S.; Ross, C. A. *Nano Lett.* **2007**, *7* (7), 2046–2050.
(59) Jeong, S. J.; Kim, J. E.; Moon, H. S.; Kim, B. H.; Kim, S. M.; Kim, J. B.; Kim, S. O. *Nano Lett.* **2009**, *9* (6), 2300–2305.
(60) Kim, S. O.; Solak, H. H.; Stoykovich, M. P.; Ferrier, N. J.; de Pablo, J. J.; Nealey, P. F. *Nature* **2003**, *424* (6947), 411–414.
(61) Han, E.; Stuen, K. O.; La, Y. H.; Nealey, P. F.; Gopalan, P. *Macromolecules* **2008**, *41* (23), 9090–9097.
(62) Schneider, C. A.; Rasband, W. S.; Eliceiri, K. W. *Nat. Methods* **2012**, *9* (7), 671–675.